pH Dependence of Peptidylglycine Monooxygenase. Mechanistic Implications of Cu−Methionine Binding Dynamics†

Andrew T. Bauman, Shula Jaron,‡ Erik T. Yukl, Joel R. Burchfiel, and Ninian J. Blackburn*

Department of Environmental and Biomolecular Systems, OGI School of Science and Engineering, Oregon Health and Sciences University, 20000 Northwest Walker Road, Beaverton, Oregon 97006-8921

Received May 7, 2006; Revised Manuscript Received June 15, 2006

ABSTRACT: The pH dependence of the PHM-catalyzed monooxygenation of dansyl-YVG was studied in two different buffer systems in the pH range of 4−10. The pH−activity profile measured in a sulfonic acid buffer exhibited a maximum at pH 5.8 and became inactive at pH >9. The data could be fit to a model that assumed a protonated unreactive species A, a major reactive species B, and a less reactive species C. B formed in a deprotonation step with pK_a of 4.6, while C formed and decayed with pK_as of 6.8 and 8.2, respectively. The pH dependence was found to be dominated by k_{cat}, with K_m(dansyl-YVG) remaining pH-independent over the pH range of 5−8. Acetate-containing buffers shifted the pH maximum to 7.0, and the activity−pH profile could be simulated by formation and decay of a single active species with pK_as of 5.8 and 8.3, respectively. The pH-dependent changes in activity could be correlated with a change in the Debye−Waller factor for the Cu−S(met) (M314) component of the X-ray absorption spectrum which underwent a transition from a tightly bound inactive "met-on" form to a conformationally mobile active "met-off" form with a pK_a which tracked the formation of the active species in both sulfonic acid and acetate-containing buffer systems. The data suggested that the conformational mobility of the bound substrate relative to the copper−superoxo active species is critical to catalysis and further suggested the presence of an accessible vibrational mode coupling Cu−S motion to the H tunneling probability along the Cu−O···H···C coordinate.

Peptidylglycine monooxygenase (PHM)[1] catalyzes the C-terminal amidation of peptides via hydroxylation of the C_α position of the peptidylglycine precursor using molecular oxygen (*1*−*3*). The catalytic core of the monooxygenase domain (PHMcc) has been studied in detail using a variety of crystallographic (*4*−*7*), spectroscopic (*8*−*15*), and kinetic (*16*−*20*) approaches. The active site is formed from two mononuclear copper centers bound to individual domains and separated by 11 Å across a solvent accessible channel as shown in Figure 1. The chemical environments around each of the copper centers are distinct. The Cu_H center (named for its histidine coordination) is bound by H107, H108, and H172 in domain 1, while the Cu_M center (named for its methionine coordination) is bound by H242, H244, and M314. EXAFS studies have shown that the coordinated methionine is lost when the enzyme is oxidized from Cu(I) to Cu(II) states (*11*). This chemistry mirrors recent discoveries of Cu(I)-binding proteins which utilize met-rich coordination sites to selectively stabilize the Cu(I) oxidation state (*21*−*25*).

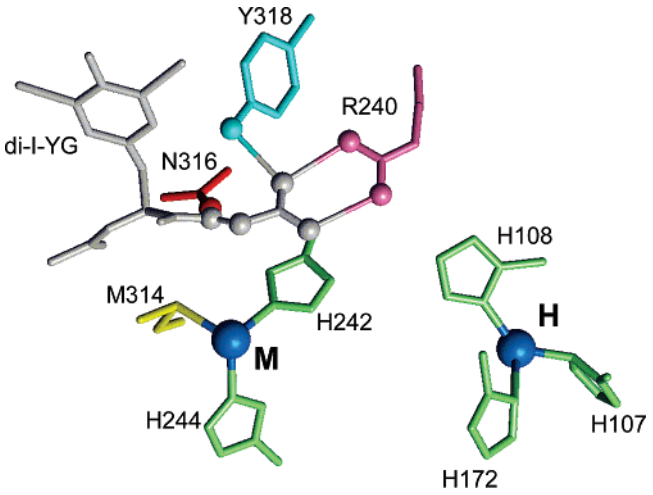

FIGURE 1: Active site of PHM showing the Cu_M site (H242, H244, and M314), the Cu_H site (H107, H108, and H172), and the bound substrate di-I-YG. Peptide substrate (gray) binds via its carboxy terminus to R240 on the same β-strand that harbors Cu_M ligands H242 and H244, but it also forms H bonds to residues Y318 and N316 on the adjacent strand that provides the M314 ligand. Coordinates were taken from PDB entry 1OPM.

The mechanism of peptidylglycine C_α hydroxylation is unique in that it is driven by donation of electrons from two mononuclear copper atoms (*3*, *10*, *26*) rather than the more

† The work was supported by a grant (R01 NS27583) from the National Institutes of Health to N.J.B.

* To whom correspondence should be addressed: Department of Environmental and Biomolecular Systems, OGI School of Science and Engineering, Oregon Health and Sciences University, 20000 NW Walker Rd., Beaverton, OR 97006-8921. Phone: (503) 748-1384. Fax: (503) 748-1464. E-mail: ninian@ebs.ogi.edu.

‡ Present address: The Lewis Center for Neuro-Imaging, University of Oregon, Eugene, OR 97403.

[1] Abbreviations: Ac-YVG, acetyl-Tyr-Val-Gly; AMP, acetate/MES/phosphate; APB, acetate/phosphate/borate; DBM, dopamine β-monooxygenase; dansyl-YVG, dansyl-Tyr-Val-Gly; DW, Debye−Waller; ET, electron transfer; EXAFS, extended X-ray absorption fine structure; KIEs, kinetic isotope effects; met, methionine; PHM, peptidylglycine monooxygenase; XAS, X-ray absorption spectroscopy.

10.1021/bi060905a CCC: $33.50
Published on Web 08/22/2006

usual coupled binuclear metal centers (*27*, *28*). Two mechanisms have been advanced in which a $Cu_M(II)$−peroxo intermediate is the active species, involving either substrate-mediated electron transfer (ET) (*4*, *5*) or superoxide channeling (*10*, *13*), but neither of these is consistent with all of the available data. Glutamine 170, a critical residue in the substrate-mediated ET pathway, can be mutated to alanine with no loss of catalytic activity (*14*), while in the related enzyme dopamine β-monooxygenase (DBM), oxygen reduction and substrate hydroxylation remain tightly coupled even in the case of extremely slow substrates, apparently ruling out superoxide channeling where some leakage of superoxide into bulk solution would be expected (*16*). An alternative mechanism which utilizes a $Cu_M(II)$−superoxo intermediate is now thought to be more likely, supported by both theoretical calculations (*26*) and kinetic studies (*16*, *29*). The $Cu_M(II)$−superoxo species is thought to extract the *pro-S* H atom of the substrate via hydrogen tunneling through an activation barrier which is moderate relative to the hydroperoxo pathway (*3*, *15*, *18*, *30*). A recent study of peptidylglycine hydroxylation using peroxide as the source of O atoms was able to rule out the Cu(II)−hydroperoxo intermediate as the active species and provided strong experimental evidence for the Cu(II)−superoxo species being the reactive entity (*29*).

Many aspects of the reaction mechanism remain obscure. Of particular interest are the absolute requirement for methionine at position 314 (*31*) and the pH dependence which maximizes at pH ~5.8. Crystal structures of the oxidized wild-type (WT) protein have been determined at pH 5.0 (*4*) and 8 (*7*); however, few structural differences are apparent at the resolution of these structures, and few detailed studies of the pH dependence of the enzyme over a broad range of pHs and buffers have been reported. In the work presented here, we present a more detailed study of the pH dependence of the activity and spectroscopy of the enzyme, using X-ray absorption (XAS) to monitor pH-dependent changes in the structure of the copper centers in the fully reduced enzyme. Our results provide a surprising link between the pH profile and the M314 ligand, showing a pH-dependent change in the mobility of the Cu−S(methionine) bond at the Cu_M center which appears to track the pH dependence of catalysis. Specifically, the enzyme exists in two distinct forms, a methionine-on form and a methionine-off form which interconvert with a pK_a of ~5. Further, the interconversion of these forms involves a conformational change of the protein which is inhibited in a frozen matrix. Surprisingly, our results implicate the met-off form as the catalytically active species. It is suggested that the met-off form provides flexible protein dynamics critical for increasing the probability of H tunneling in the rate-determining step.

MATERIALS AND METHODS

All buffers as well as the ascorbic acid were obtained from Sigma-Aldrich at a minimum purity of 99%. Beef liver catalase was acquired from Roche. The Ac-Tyr-Val-Gly (Ac-YVG) peptide was provided by Peptide International, and dansyl-Tyr-Val-Gly (dansyl-YVG) was from American Peptide Co. PHM was isolated and purified from a CHO cell line as previously described (*29*). The purified enzyme was reconstituted with cupric sulfate by slow addition of 2.5 molar equiv followed by exhaustive dialysis against 20 mM sodium phosphate buffer (pH 8.0) containing 25 μM Cu(II) ion. The reconstituted enzyme was concentrated by ultrafiltration to approximately 4 mM in Cu(II) and used immediately. Protein concentrations were determined using the OD_{280} on a Shimadzu UV-265 spectrophotometer at ambient temperature using an extinction coefficient for a 0.1% solution at 280 nm of 0.980. Copper concentrations were determined using a Perkin-Elmer Optima 2000 DV inductively coupled plasma optical emission spectrometer.

Buffer Systems. The following sulfonic acid buffers were used: MES [2-(1-morpholino)ethanesulfonic acid], PIPES [1,4-piperazinebis(ethanesulfonic acid)], HEPES [4-(2-hydroxyethyl)-1-piperazineethanesulfonic acid], HEPBS [*N*-(2-hydroxyethyl)piperazine-*N*′-(4-butanesulfonic acid)], and CHES [2-(cyclohexylamino)ethanesulfonic acid]. These were made at concentrations of 50 mM and brought to the appropriate pH using sodium hydroxide. The combined buffer systems, AMP (acetate/MES/phosphate) and APB (acetate/phosphate/borate), were 50 mM in each of their respective components and were brought to the appropriate pH using the same method. Catalase was diluted by a factor of 5 in 50 mM phosphate buffer (pH 7.5). Purified PHM was also diluted in this buffer to an average concentration of 0.5 mg/mL. The exact concentration was determined by OD_{280} measurements.

Measurements of Reaction Rates. Kinetic experiments assessing O_2 consumption were performed using a Rank Brothers LTD model 10 electrode with the polarizing voltage set to 630 mV. The water-jacketed reaction cell was kept at 37 °C using a circulating constant-temperature water bath. The electrode was calibrated by purging the solution of oxygen with argon and adjusting the output to 100% for oxygen-saturated water at 37 °C. The water was removed, and 1.59 mL of the appropriate buffer, stored in the constant-temperature bath, was added to the cell that was being stirred. This was followed by 200 μL of a 2.5 mg/mL catalase solution. Next, 100 μL of a 100 μM Cu^{2+} solution was added followed by 2−10 μL of ~0.5 mg/mL PHM. A cap was then placed over the cell. After an equilibration time of approximately 1 min, 30 μL of 25 mM Ac-YVG substrate in methanol was injected through the cap to initiate the reaction. The oxygen consumption was monitored by a computer interfaced with the electrode, taking data every 1 s.

The initial reaction rate was taken to be the slope of the linear portion of the electrode output versus time plot for each run. The concentration of oxygen-saturated water was taken to be 214 μM in O_2. At each pH that was measured, four replicates of five different enzyme concentrations were run. The validity of the data was assessed by plotting the initial rate versus enzyme concentration. These plots were linear with R^2 values never below 0.99. The uncatalyzed rate was taken to be the *y*-intercept of these plots.

The buffer systems were chosen so that the accessible pHs of each buffer overlapped with another buffer on each side of the pH range. In these overlap regions, rate measurements were taken at identical pHs in each of the two buffers to check for buffer-specific effects on the V_{max} values. Differences in rates were used to normalize the data, using a correction factor which was typically small. The largest correction factors were observed for the overlap between HEPBS and CHES at pH 9.0 (0.439) and between AMP and APB at pH 8.0 (1.53). Values of V_{max} versus pH with

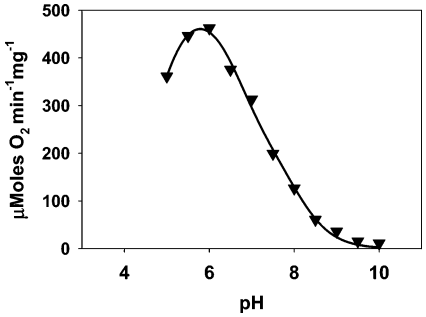

FIGURE 2: pH−activity profile for the PHM reaction in the sulfonic acid buffer system. The solid line represents a fit to the data assuming the formation of active species B with a pK_a of 4.7, which converts to a less active form C with a pK_a of 6.7. C converts to an inactive form with a pK_a of 8.1.

normalization factors are listed for each buffer system in Tables S1 and S2 of the Supporting Information.

Steady State Kinetic Measurements. The pH dependence of kinetic constants K_m and V_{max} was determined at 25 °C using HPLC to separate and quantify substrate and product. Reverse phase HPLC was performed with a Varian Pro Star solvent delivery module equipped with a Varian Pro Star model 410 autosampler (250 μL syringe, 100 μL sample loop), on a 250 mm × 4.6 mm Varian Microsorb-MV 100-5 C18 column. Substrate (dansyl-YVG) and product (produced by the PHM-catalyzed reaction) were monitored by their dansyl fluorescence using a Waters 474 scanning fluorescence detector (λ_{ex} = 365 nm; λ_{em} = 558 nm). Solvent A was 0.1% trifluoroacetic acid (TFA) in water, and solvent B was 0.1% TFA in acetonitrile. Product was separated from substrate via isocratic loading and elution at 25% solvent B in solvent A.

Reaction rates were determined by following the rate of substrate consumption (or product formation) as a function of time. The reaction was performed in a water-jacketed glass reaction vessel, with stirring, in 100 mM sulfonic acid buffer [MES, PIPES, and HEPES (pH 5−8)] at 25 °C. All reagents, except dansyl-YVG, were added to the following final concentrations: Cu^{2+} as copper sulfate (5 μM), catalase (250 μg), ascorbate (10 mM), and PHM (2.5−5 μM). After the reagents were allowed to incubate for 2 min, the reaction was initiated by adding dansyl-YVG from a 25 mM stock, to a final concentration of 10−100 μM. In a typical experiment, 330 μL aliquots were removed every 30 s, transferred to a 1.5 mL microcentrifuge tube containing 10 μL of 10% TFA, and vortexed for 10 s. Substrate and product were separated by HPLC, and their concentrations were determined using a standard curve built from chromatograms of 10−200 μM samples of dansyl-YVG run under identical conditions. Kinetic constants were extracted from the raw data by fitting to the Michaelis−Menten equation using nonlinear regression in Sigmaplot version 8.0.

Simulation of Reaction Rate Data. The model which best fit the data of Figure 2 assumes that at least four species interconvert by protonation equilibria. Species A is inactive and converts into active species B, with association constant K_A. B converts to a less active form C with association constant K_B. C is further converted into inactive form D with association constant K_C. The rate constant can be written

$$k_{cat} = k_1[B] + k_2[C] \quad (1)$$

Using mass action and mass balance equations to solve for the concentration of B and C, we obtain (see the Supporting Information for full derivation)

$$k_{cat} = \frac{k_1 K_B[H]}{1 + K_B[H] + K_A K_B[H]^2} + \frac{k_2 K_C[H]}{1 + K_C[H] + K_B K_C[H]^2} \quad (2)$$

Values of k_{cat} (micromoles of O_2 per minute per milligram) were plotted against pH and fitted to eq 2 by nonlinear regression using Sigmaplot version 8.0. Values of K_A, K_B, K_C, k_1, and k_2 were refined.

Data in AMP and APB buffer systems could be fit to a simpler rate equation involving a single reactive species, B′, which is clearly different from B

$$k'_{cat} = k_3[B'] \quad (3)$$

Solving for [B′] gives

$$k'_{cat} = \frac{k_3 K'_B[H]}{1 + K'_B[H] + K'_A K'_B[H]^2} \quad (4)$$

Values of k'_{cat} (micromoles of O_2 per minute per milligram) were plotted against pH and fitted to eq 2 by nonlinear regression using Sigmaplot version 8.0. Values of K'_A, K'_B, and k_3 were refined.

Measurement of Dansyl-YVG Dissociation Constant K_d. For the oxidized enzyme, an Amicon (5 mL) ultrafiltration device was first preincubated overnight with 300 μM Cu(II)-loaded PHM (2.0 Cu atoms per protein) in either 100 mM MES (pH 5.5) or 100 mM HEPES (pH 8.0) containing 1 mM dansyl-YVG. The protein solution was then washed repeatedly with buffer until the substrate concentration in the filtrate had fallen to a low level as determined by measurement of the dansyl fluorescence of the filtrate. This conditioning procedure ensured that all irreversible substrate and/or protein binding sites on the membrane were occupied. Next, dansyl-YVG was titrated into the PHM solution, and aliquots of the filtrate were extracted for analyses as follows. A septum was placed over the ultrafiltration cell, and the cell was pressurized by injecting 0.6 mL of air over the solution. After a small amount of filtrate had been collected, it was returned to the concentrator and the process repeated three times. On the fourth pressurization, 10 μL of filtrate was saved for analysis of the concentration of the "free" substrate by fluorimetry (λ_{ex} = 365 nm; λ_{em} = 558 nm). The remaining filtrate was returned to the concentrator along with the next titration aliquot (30 μL) of 10 mM substrate for a net volume gain of 20 μL. This procedure was repeated until a total substrate concentration of 1 mM was reached.

For the reduced protein, the following modifications to the procedure were used. All solutions were first purged with Ar and placed in an anaerobic chamber. Cu(II)-loaded PHM (2.0 Cu atoms per protein) in 100 mM sulfonic acid buffer [MES (pH 5.0 and 6.0) or HEPES (pH 7.0 and 8.0)] was reduced with a 5-fold excess of buffered ascorbate and then

titrated with dansyl-YVG in a conditioned ultrafiltration cell in the anaerobic chamber using an identical protocol.

The data were analyzed by constructing plots of fractional binding, f, [=([S_T] − [S_F])/[E_T]] versus free substrate S_F (where the subscripts T and F represent total and free, respectively). These data were fit by nonlinear regression (Sigmaplot version 8.0) to the equation

$$f = \frac{nS_F}{K_d + S_F}$$

where K_d is the dissociation constant for binding of dansyl-YVG to PHM and n is the number of binding sites. Values of K_d and n were refined in the fits. Values of n were found to range between 1.1 and 1.3, where the deviation from 1 probably represents inaccuracies in protein concentration, irreversible binding effects, nonideality, and nonequilibrium membrane effects.

Preparation of Samples for XAS. All solutions were first made anaerobic, and all manipulations were carried out in the anaerobic chamber. Samples for XAS were prepared in a single step by dilution of a 20 μL volume of 2 mM oxidized PHM [4 mM in Cu(II), 20 mM sodium phosphate (pH 8.0)], with 80 μL of the appropriate buffer containing 5 mM ascorbate and 25% ethylene glycol. After the sample had been transferred to the XAS cuvette, the sample was flash-frozen by rapid immersion in liquid nitrogen.

Collection and Analysis of XAS Data. Cu K-edge (8.9 keV) extended X-ray absorption fine structure (EXAFS) and X-ray absorption near-edge structure (XANES) data were collected at the Stanford Synchrotron Radiation Laboratory operating at 3 GeV with currents between 100 and 50 mA. All samples were measured on beam line 9-3 using a Si[220] monochromator and a Rh-coated mirror upstream of the monochromator with a 13 keV energy cutoff to reject harmonics. A second Rh mirror downstream of the monochromator was used to focus the beam. Data were collected in fluorescence mode using a high-count rate Canberra 30-element Ge array detector with maximum count rates below 120 kHz. A 6 μm Z-1 Ni oxide filter and Soller slit assembly were placed in front of the detector to reduce the elastic scatter peak. Six scans of a sample containing only sample buffer were collected at each absorption edge, averaged, and subtracted from the averaged data for the protein samples to remove Z-1 K_β fluorescence and produce a flat pre-edge baseline. The samples (80 μL) were measured as aqueous glasses (>20% ethylene glycol) at 10 K. Energy calibration was achieved by referencing the first inflection point of a copper foil (8980.3 eV) placed between the second and third ionization chamber. Data reduction and background subtraction were performed using the program modules of EXAFSPAK (*32*). Data from each detector channel were inspected for glitches or drop-outs before inclusion in the final average. Spectral simulation was carried out with EXCURVE version 9.2 (*33*−*36*) as previously described (*11*).

Photoreduction experiments were carried out by exposing a sample of oxidized PHM to the X-ray beam at 100 K. The slits were opened during the photoreduction process to illuminate a sample spot of 10 mm × 2 mm. Alignment of the beam relative to the optical table was performed with the shutter closed between the I_0 ion chamber and the sample cryostat to minimize photoreduction prior to collection of the $t = 0$ absorption edge spectrum. Absorption edge spectra (8960−9020 eV range) were measured at 30 min time intervals during the photoreduction process, using a rapid edge scanning procedure which collected data at 0.5 eV energy intervals for 1 s per point. Reduction was monitored from the increase in intensity at 8983 eV and was continued until no further change in F/I_0 was observed at this energy. Rate constants for photoreduction were calculated by fitting to the equation

$$(F/I_0)_{8983}^{t=t} - (F/I_0)_{8983}^{t=0} = A(1 - e^{kt})$$

where $(F/I_0)_{8983}^{t=t}$ and $(F/I_0)_{8983}^{t=0}$ represent the 8983 eV fluorescence intensity at time t and time 0, respectively, and k is the rate constant. After photoreduction was complete, the slits were closed to 5 mm × 1 mm, and the temperature was returned to 10 K. Four EXAFS scans were then collected.

For each pH and buffer system, EXAFS data were simulated using a two-shell model for Cu(I)−imidazole coordination as previously described (*11*−*13*). Fits were obtained by first fixing the imidazole ring geometry to an ideal value and refining the first-shell distance (R) and Debye−Waller factor for the two Cu−N(imid) shells (including the single and multiple scattering contributions for the imidazole rings), the Cu−S(met) shell, and E_0. In these preliminary refinements, the imidazole ring outer shell C and N atoms were constrained to move relative to the first-shell Cu−N distance so the idealized ring geometry could be maintained. Later in the refinement, this constraint was lifted, and the outer shells of the imidazole rings were allowed to float within 10% of their original idealized positions. In practice, final outer shell coordinates deviated by less than the permitted amount from the idealized position. In some fits, the Cu−S(met) coordination number was fixed at 0.57, and the DW of this shell refined. In other fits, the DW factor was fixed at 0.0010 Å^2 and the Cu−S coordination number was refined. In general, the former procedure gave better fits to the data.

Cu−S(met) DW factors were plotted versus pH for each buffer system and fitted to the equation

$$\mathrm{DW} = A + \frac{B}{1 + K_A[\mathrm{H}]}$$

where $A = \mathrm{DW}_{min}$ (the DW factor for the fully met-on form) and $B = (\mathrm{DW}_{max} - \mathrm{DW}_{min})$ (the difference between DW factors for the met-on and met-off forms).

RESULTS

The pH dependence of the catalytic activity (k_{cat} vs pH) was determined first in a mixed buffer system composed of a series of noncoordinating sulfonic acid buffers (MES, HEPES, PIPES, HEPBS, and CHES) with overlapping pH ranges to allow for adjustments in catalytic rates due to buffer-dependent effects. This system provided good buffering capacity between pH 5 and 10. We also determined the pH dependence of PHM catalysis in a second buffer system made up of 50 mM acetic acid, 50 mM MES, and 50 mM sodium dihydrogen phosphate (AMP). To access pH values of ≥9, MES was replaced with 50 mM sodium borate to give a buffer composition of 50 mM acetate, 50 mM

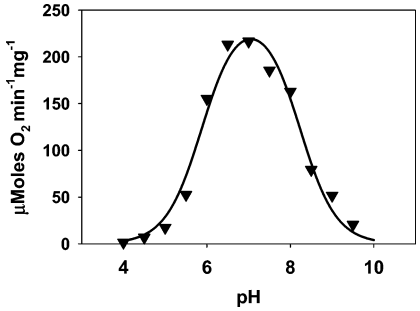

FIGURE 3: pH−activity profile for the PHM reaction in the acetate-containing buffer system. The solid line represents a fit to the data assuming the formation of active species B with a pK_a of 5.9, which converts to an inactive form with a pK_a of 8.2.

phosphate, and 50 mM borate (APB). These buffer systems enabled measurement of rates at pH values as low as 4.0 due to the buffering capacity of the acetate and acetic acid and also provided information about buffer ion-dependent changes in activity.

Figures 2 and 3 show V_{max} versus pH data for the sulfonic acid buffer system and the AMP/APB system, respectively. It is evident that the profiles are not identical. Specifically, the rate curve in the acetate-containing AMP buffer is shifted to a higher pH, and the maximum rate in MES at pH 7 is approximately half that in MES at pH 6. It is unclear whether this effect is due to mild inhibition by a component of the AMP buffer system, ionic strength effects, or both. Analysis of the differences in rate showed that the primary difference was due to the acetate component in the buffer system. In the following sections, the buffer systems giving rise to the data in Figures 2 and 3 are therefore termed sulfonic acid and acetate-containing, respectively.

We simulated the pH dependence in both buffer systems using the following assumptions (for full details, see Materials and Methods). The rate versus pH profiles have an activation phase in which the rates increase with pH, followed by a deactivation phase in which the rates decrease with pH. Simulations which assumed a simple single deprotonation for both activation and deactivation were in good agreement with the data for the acetate-containing buffer system but were insufficient to describe the sulfonic acid system. The acetate-containing system could be simulated by an activation phase with pK_a of 5.9 ± 0.1 and a deactivation phase with a pK_a of 8.2 ± 0.1. The sulfonic acid system could be simulated by a single activation phase with a pK_a value of 4.7 ± 0.1 and two deprotonations in the deactivation phase with pK_a values of 6.7 ± 0.2 and 8.1 ± 0.2, respectively (Table 1).

Kinetic constants (K_m and k_{cat}) were determined as a function of pH for the sulfonic acid buffer system (Table 2). Over the pH range of 5−8, the apparent K_m for the substrate dansyl-YVG decreased with an increase in pH until at pH 8 it was too small to measure using HPLC detected by the fluorescence of the dansyl group. A decrease in the level of substrate binding with an increase in pH is not expected since the substrate H bonds to the protonated Y318 (Figure 1), which should begin to ionize around pH 8. Thus, we suspected that the apparent decrease in K_m might be due to a change in the rate-limiting step from substrate hydroxylation to ascorbate reduction as the pH increased. To further address the issue, we measure the pH dependence of K_d for

Table 1: Acid Association Constants for the Protonation of Catalytically Active Forms of PHM[a]

	sulfonic acids	acetate	Cu−S DW sulfonic acids	Cu−S DW acetate
k_1	527 ± 24			
k_2	190 ± 10			
k_3		249 ± 14		
log K_A	4.7 ± 0.1		4.8 ± 0.3	
log K_B	6.7 ± 0.2			
log K_C	8.1 ± 0.2			
log K'_A		5.9 ± 0.1		5.9 ± 0.13
log K'_B		8.2 ± 0.1		

[a] In the sulfonic acid buffer system, data were fit to a model which assumes an inactive form A converting to active forms B and C with rate constants k_1 and k_2 and association constants K_A, K_B, and K_C, respectively. In acetate-containing buffers, the data were fit to a model which assumes an inactive form A′ converting to an active form B′ with rate constant k_3 and acid association constants K'_A and K'_B, respectively.

Table 2: pH Dependence of Dissociation Constant K_d for Binding of Dansyl-YVG to the Oxidized and Reduced Forms of PHM Compared with That of Michaelis Constant K_m

pH	K_m (μM)	K_d(reduced) (μM)	K_d(oxidized) (μM)
5.0	6.6 ± 1.0	2.9 ± 1.0	
5.5	7.2 ± 1.0		145.4 ± 16
6.0	3.0 ± 0.8	5.4 ± 1.2	
7.0	0.91 ± 0.3	4.0 ± 1.3	
8.0	not measurable	3.1 ± 0.9	131 ± 10

binding of substrate to the oxidized and reduced proteins in the pH range of 5−8. The results (Table 2) showed that K_d was invariant with pH over this range but varied with the oxidation state of the copper center as previously reported (*29*). For the reduced enzyme, $K_d = 4 \pm 2$ μM, while for the oxidized enzyme, $K_d = 140 \pm 10$. The value for the reduced enzyme is identical to the K_m measured in MES at pH 5.5 which implies that all steps in the reaction up to substrate binding are reversible. Further, since K_d does not decrease with pH, it also suggests that pH-dependent effects on K_m are due to a transition to zero-order (i.e., non-rate-limiting) kinetics for the disappearance of substrate. This further suggests that the variation of rate with pH is due entirely to k_{cat}.

The crystal structure of PHMcc has been determined for the oxidized, reduced, and di-iodo-YG-bound oxidized forms (*2*, *4*, *5*, *7*) at pH 5 and 8. No obvious candidates for active site acids or bases are apparent from the structures, except perhaps copper-coordinated imidazole or water molecules. To probe these possibilities, we examined the X-ray absorption spectra of the oxidized and reduced proteins in the pH range of 4−9 in the presence and absence of the substrate dansyl-YVG. A complicating factor in assessing the pH dependence of the coordination environment of the copper centers was the possibility that the affinity of the enzyme for copper might weaken as the pH is lowered, and we therefore measured copper loading as a function of pH. Samples were fully loaded with cupric ion at pH 8 in 20 mM sodium phosphate buffer to give Cu^{2+}/protein ratios of 2.0−2.2. The samples were made anaerobic and then rapidly diluted with a 5-fold excess of anaerobic pH buffer which contained five reducing equivalents of sodium ascorbate per copper. Although no copper was removed from the system during this procedure, copper loss could still occur if Cu(I)

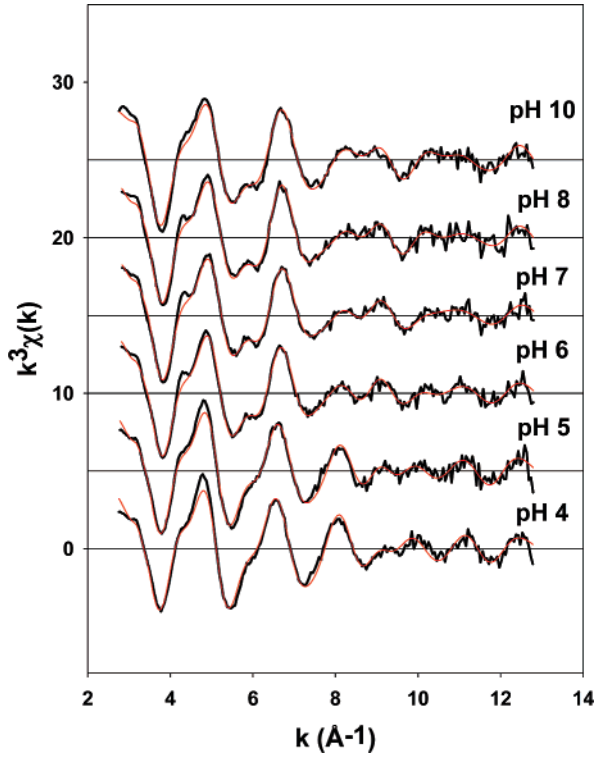

FIGURE 4: Experimental (black) vs simulated (red) EXAFS spectra for ascorbate-reduced PHM as a function of pH in the acetate-containing buffer system. Traces were recorded at pH 4, 5, 6, 7, 8, and 10.

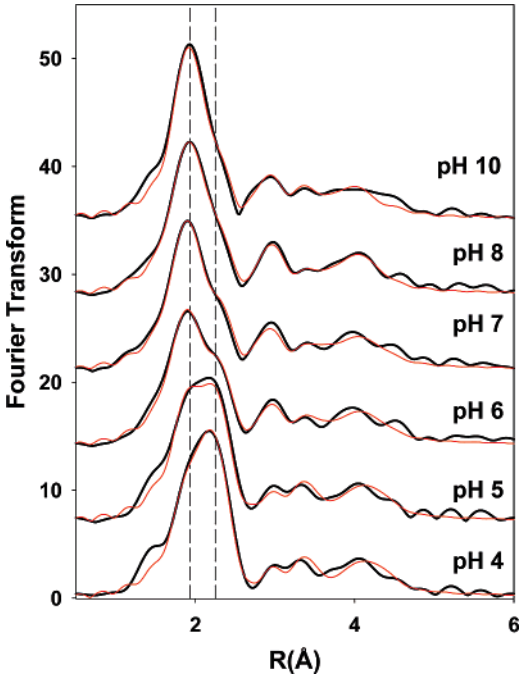

FIGURE 5: Experimental (black) vs simulated (red) Fourier transforms (corrected for the Cu−N phase shift) for ascorbate-reduced PHM as a function of pH in the acetate-containing buffer system. Traces were recorded at pH 4, 5, 6, 7, 8, and 10. Vertical dashed lines show the position of the Cu−N (1.98 Å) and Cu−S shells (2.25 Å).

dissociated and disproportionated to Cu(II) and Cu(0), where the latter could "plate out" onto the walls of the container. Measurement of copper/protein ratios after dilution gave values that were essentially unchanged above pH 6 and never dropped below 1.8 even at the lowest pH, indicating that copper loss was insignificant. EXAFS and EPR of the oxidized enzyme (data not shown) were invariant in the pH range of 5−7.5 and were not studied further. EXAFS of the reduced protein, however, showed interesting pH-dependent changes.

The EXAFS of reduced PHM has been reported in previous papers from this laboratory (*8*, *10*, *11*). The important features of these previous simulations included splitting of the copper−histidine shell into two sets of scatterers: one for which $R = 1.88$ Å and a second for which $R = 1.98$ Å. This splitting was justified on the basis that the single-shell Cu−His fits gave high Debye−Waller factors, and it was already known from crystallography that the two sites were structurally distinct. Analysis of two mutant proteins (M314I and H242A) in which copper was absent from the M center confirmed the short distance [typical of two-coordinate Cu(I)] and assigned it to the reduced Cu_H site. A second feature of the Cu(I) spectra was a component due to Cu−S(met) scattering at $R = 2.24$ Å. For spectra measured in phosphate buffer at pH 7.5, the Debye−Waller factor for the Cu−S shell was unusually high with values in the range of 0.009−0.012 Å^2.

In this study, EXAFS data were measured for the acetate and sulfonic acid buffer systems as a function of pH. Spectra were simulated using the split histidine shell model. Figures 4 and 5 show EXAFS and Fourier transforms for the acetate-containing buffer system. A significant spectral change is observed as the pH is increased. The vertical lines in the FTs are positioned at the distances corresponding to the Cu−His and Cu−S(met) shells, respectively, and emphasize that at pH 4 the Cu−S(met) component is intense and dominates the first shell while at pH 9 the Cu−S(met) interaction has all but disappeared. Simulation of the data allows this observation to be quantified using the parameters listed in Table 3 (a complete list of parameters used in the fits is supplied as Table S3 of the Supporting Information). The spectral changes can be almost completely ascribed to a change in the Cu−S Debye−Waller (DW) factor from 0.0010 Å^2 at pH 4 to 0.0120 Å^2 at pH 9. The change in the Cu−S DW factor is plotted as a function of pH in Figure 6. The curve can be simulated well by a single deprotonation event with a pK_a of 5.9 ± 0.13.

The absorption edges of the acetate spectra in the pH range of 4−8 are shown in Figure 7. The intensity of the 8983 eV edge feature increases and moves slightly to a higher energy as the pH is increased, and these changes track the same pH-dependent transition that was observed for the Cu−S DW factor. From Table 3, it can be seen that the Cu−N bond length for one of the His ligands sets is shortened by 0.05 Å over this same pH transition from 1.90 to 1.85 Å, which together with the increase in 8983 eV intensity would be consistent with this set of histidines becoming more two-coordinate (*37*−*39*). As discussed above, our previous EXAFS studies at pH 7.5 of the H242A mutant of PHM which lacks the Cu_M center suggested a two-coordinate structure from which we assigned the short Cu−N(His) distance to the Cu_H His residues (*11*). The more recent X-ray structure of the M314I variant (*7*) showed that the H107 ligand at Cu_H was disordered with only 30% occupancy, establishing an unexpected structural relationship between the two copper centers. These observations suggest a provocative interpretation of the edge spectra, that the pH-

Table 3: Fits to the EXAFS of PHM in AMP Buffer Obtained by Curve Fitting Using EXCURVE Version 9.2

		Cu−S			C−N(His)[b]			Cu−N(His)[b]			
pH	F[a]	no.[c]	R (Å)[d]	DW (Å^2)	no.[c]	R (Å)[d]	DW (Å^2)	no.[c]	R (Å)[d]	DW (Å^2)	$-E_0$
4.0	0.258	0.6	2.259	0.001	1 N	2.006	0.001	1 N	1.900	0.010	1.77
5.0	0.330	0.6	2.255	0.003	1 N	1.998	0.001	1 N	1.879	0.010	1.33
5.5	0.259	0.6	2.250	0.005	1 N	1.982	0.001	1 N	1.857	0.006	0.59
6.0	0.237	0.6	2.250	0.009	1 N	1.972	0.001	1 N	1.848	0.005	0.56
7.0	0.217	0.6	2.241	0.012	1 N	1.964	0.001	1 N	1.846	0.005	0.32
8.0	0.274	0.6	2.232	0.012	1 N	1.970	0.001	1 N	1.850	0.005	0.45
10.0	0.234	0.6	2.239	0.012	1 N	1.979	0.001	1 N	1.871	0.005	1.74

[a] F is a least-squares fitting parameter defined by the equation $F^2 = 1/N \sum_{i=1}^{N} k^6(\text{data} - \text{model})^2$. [b] Fits modeled histidine coordination by an imidazole ring, which included single and multiple scattering contributions from the second-shell (C2 and C5) and third-shell (C3 and N4) atoms, respectively. The Cu−N−C$_x$ angles were as follows: 126° for Cu−N−C$_2$, −126° for Cu−N−C$_3$, 163° for Cu−N−N$_4$, and −163° for Cu−N−C$_5$. [c] Coordination numbers are generally considered accurate to ±25%. [d] In any one fit, the statistical error in bond lengths is ±0.005 Å. However, when errors due to imperfect background subtraction, phase shift calculations, and noise in the data are compounded, the actual error is probably closer to ±0.02 Å. All fits included an additional shell of two single scattering C atoms at 3.3 Å. We speculate that these C atoms derive from the methyl and methylene C shells of the met ligand and from the methylene C atoms of the Nδ-coordinated histidines at Cu$_H$.

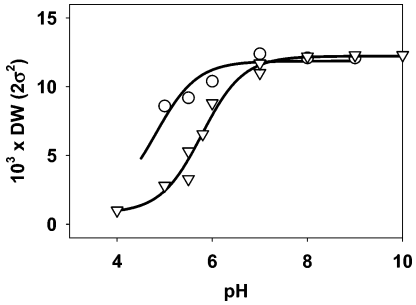

FIGURE 6: pH dependence for the Cu−S Debye−Waller factor. Triangles represent data for the acetate-containing buffer system and circles data for the sulfonic acid-containing buffer system. The solid lines represent single deprotonation titration curves with pK_a values of 5.9 and 4.8.

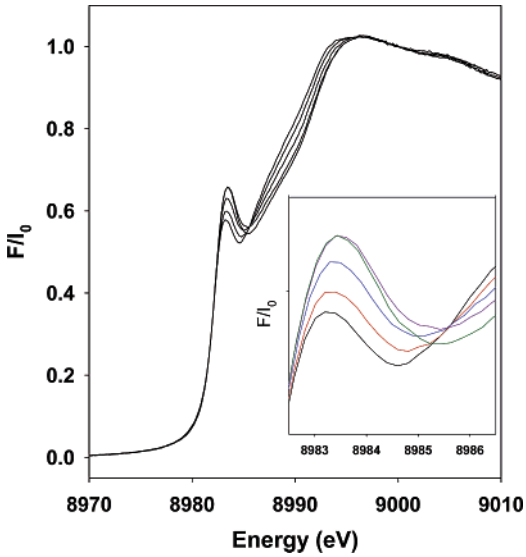

FIGURE 7: Absorption edges for reduced PHM in acetate-containing buffer. Spectra were recorded at pH 4, 5, 5.5, 6, and 8. Edges were normalized at 9000 eV. The inset shows an expanded view of the 8983 eV region of the spectra.

dependent structural changes that induce the increase in the Cu−S(M314) DW factor may lead to weakening of one Cu−His interaction at the Cu$_H$ center.

The pH dependence of the EXAFS spectra measured in the sulfonic acid buffer system does not show such a dramatic spectral change. When these data were simulated using the same methodologies, the Cu−S DW factor changed from 0.008 Å^2 at pH 5.0 to 0.012 at pH 9. (These values were obtained using a Cu−S shell occupancy of 0.63 which led to DW factors equivalent to those found for the acetate system at pH 9 with a Cu−S occupation number of 0.57.) This pH dependence is also plotted in Figure 6. The shape of the curve suggests that the Cu−S DW factor in sulfonic acid buffers is likewise modulated by a deprotonation event but with a pK_a that is shifted downward by ~1 pH unit. Although the titration curve is incomplete due to the inaccessibility of pHs below 5 in this buffer system, simulation gives a pK_a of 4.8 for the transition (a complete list of parameters used in the EXAFS fits in sulfonic acid buffers is supplied as Table S4 of the Supporting Information).

Table 4: Variation of the Cu−S Debye−Waller Factor or the Cu−S Coordination Number with pH[a]

	fixed coordination number			fixed Cu−S Debye−Waller		
pH	N(Cu−S)	DW(Cu−S)	F	N(Cu−S)	DW(Cu−S)	F
4.0	0.57	0.0010	0.258	0.57	0.0010	0.258
5.0		0.0028	0.330	0.53		0.371
5.5		0.0053	0.259	0.44		0.366
6.0		0.0088	0.236	0.34		0.375
7.0		0.0117	0.217	0.30		0.334
8.0		0.0122	0.273	0.30		0.421
10.0		0.0123	0.234	0.32		0.390

[a] Fits to the EXAFS data were performed either by fixing N and floating the DW factor or by fixing the DW and floating N.

Since DW factors and coordination numbers are correlated, we tested whether the change in Cu−S shell intensity could be modeled by a decrease in Cu−S shell occupancy. With the DW term fixed at 0.0010 Å^2, reasonable fits could be obtained for the acetate-containing spectra with Cu−S coordination numbers of 0.57 at pH 4 decreasing to 0.30 at pH >7. These fits were both qualitatively and quantitatively inferior (Table 4). Additionally, in no case did the Cu−S shell occupancy decrease to zero, which would be expected if the pH transition involved a simple dissociation of the Cu−S(met) ligand.

The enzyme thus appears to exist in two forms which differ in the magnitude of the DW factor for the Cu−S(met) shell. We term these forms the met-on and met-off forms, respectively. There is some indication that one of the His residues at the Cu$_H$ center is dissociated in the met-off form. When the pK_a values for the met-on to met-off transitions

are compared with the pK_a values of the activation phases of the rate data (Table 1), the agreement is remarkable. Particularly compelling is the fact that the structural change that causes the shift in pK_a for activation between the two buffer systems produces an identical shift in the pK_a for the met-on to met-off transition. The surprising result that follows from this observation is that the met-off form of the enzyme is the active form.

XAS data measured in the presence of dansyl-YVG (data not shown) indicate that substrate binding has no effect on the position of the met-on to met-off equilibrium. This rules out the possibility that substrate locks the protein into one conformation or the other.

The data do not provide any insight into what groups are involved in the pH-dependent structural transitions. The effect either could be localized to the coordination sphere of the Cu_M center or could arise from a more global conformational change in the protein matrix. We designed an experiment to examine these scenarios as follows. The fully oxidized enzyme was photoreduced in the X-ray beam at 100 K and pH 5.1 in acetate-containing buffer. From our experiments described above, we have shown that ascorbate reduction in the same buffer in aqueous solution produces the met-on form. Oxidized Cu(II)-bound PHM has been shown previously to show no contribution from the methionine ligand in the EXAFS (*11*), due to its probable coordination in an axial position with a bond length in excess of 2.5 Å (*11*, *15*). Thus, the oxidized enzyme is in a different met-off form which does not appear to change with pH. If the met-on to met-off transition observed in the reduced protein involves only local changes at the Cu_M center, then the met-on form should be formed at pH 5.1 even in the frozen state. If, on the other hand, the met-on to met-off transition requires a global conformational change in the protein structure, this should be inhibited in the frozen state, and a met-off form should result from photoreduction at pH 5.1. The results are shown in Figure 8. The fully oxidized enzyme can be photoreduced cleanly at 100 K in a single-exponential process corresponding to pseudo-first-order kinetics, with a rate constant of 6×10^{-4} s^{-1}. The single exponential and the isosbestic point observed at 8992.5 eV indicate that a single species of reduced enzyme is formed. Analysis of the EXAFS of the fully photoreduced protein shows that the solvent scatterers present in the EXAFS of the oxidized protein have dissociated, implying that local changes in the Cu_M coordination sphere can still occur in the frozen matrix. However, the Cu−S distance is 2.25 Å when $2\sigma^2 = 0.012$ Å^2, i.e., the form corresponding to the met-off form, rather than the met-on form predicted from enzyme reduced by ascorbate in aqueous solution. This result suggests that the Cu−S interaction changes from its undetectable position in the fully oxidized protein to a position corresponding to the met-off form. The transition from met-off to met-on is inhibited in the fully reduced frozen protein at pH 5.1, suggesting that the latter requires a conformational change involving more global elements of protein structure, which are frozen out at 100 K (a complete list of parameters used in the fit to the photoreduced data is supplied as Table S5 of the Supporting Information).

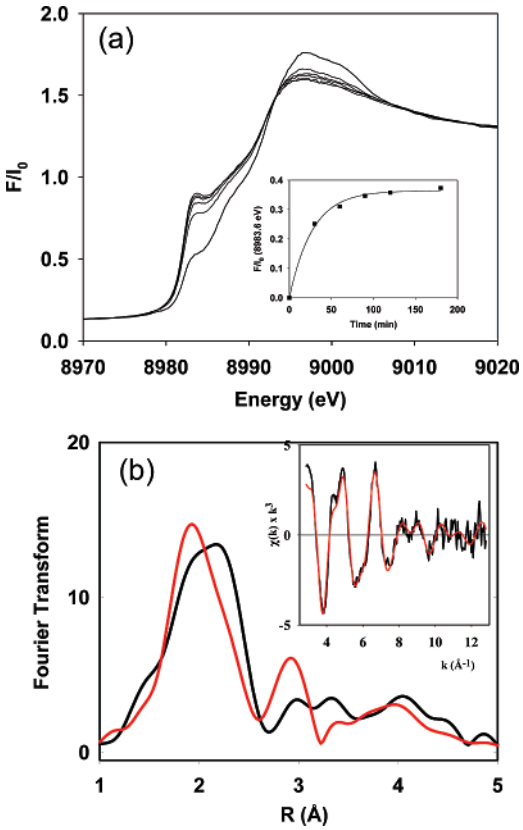

FIGURE 8: Photoreduction of oxidized PHM at 100 K. (a) Absorption edges measured at (from bottom to top) 0, 30, 60, 90, 120, and 180 min. The inset shows a first-order plot of the intensity at 8983 eV vs time with a rate constant of 6×10^{-4} s^{-1}. (b) Comparison of Fourier transforms of photoreduced (red) and ascorbate-reduced PHM at pH 5.1. The inset shows experimental (black) vs simulated (red) EXAFS for the photoreduced sample. The simulations give parameters characteristic of the met-off form.

DISCUSSION

We have studied the pH dependence of the PHM-catalyzed monooxygenation of dansyl-YVG which forms the peptidyl α-hydroxyglycine product. The pH−activity profile measured in sulfonic acid buffer systems (MES, PIPES, and CHES) increases to a broad maximum between pH 5.5 and 6 and then declines, becoming essentially inactive above pH 9. The profile implies that a deprotonation event with a pK of <6 leads to activation of the enzyme while further deprotonation steps with pK values of >6 convert the active species to a less active state. The data could be fit well to a model that assumed a protonated unreactive species A, a major reactive species B, and a less reactive species C. Active species B formed in a deprotonation step with a pK_a of 4.7, while less reactive species C formed and decayed with pK_a values of 6.8 and 8.2, respectively. The pH dependence of the rate was found to be dominated by k_{cat}, with K_m(dansyl-YVG) remaining pH-independent over the range of 5−8. Acetate-containing buffers shifted the pH maximum from 5.8 to 7. In a 50 mM mixed acetate/MES/phosphate buffer system, the activity−pH profile could be simulated by formation and decay of the active species with pK_a values of 5.8 and 8.3, respectively.

To understand the mechanistic significance of the pH−rate data, we determined the pH dependence of a number of spectroscopic markers in both the reduced and oxidized forms. The oxidized enzyme was monitored by EPR and

XAS and revealed no major changes in spectral features in the pH range of 5−7.5. The reduced form of the enzyme, however, exhibited an interesting trend in the value of the DW factor of the Cu−S(met) interaction in the Cu(I) XAS. In the acetate/MES/phosphate buffer system, the Cu−S DW factor underwent a transition from a value typical of a tightly bound Cu−S(met) form where $2\sigma^2 \leq 0.001$ Å^2 to a value typical of a weakly bound form where $2\sigma^2 \geq 0.012$ Å^2. We term these the "met-on" and "met-off" forms present at low and high pH, respectively. Very significantly, the pK_a for the transition was 5.9, identical within experimental error to that for the formation of the active species in the acetate-containing buffer system. This strongly suggests that the met-off form is the active species. In support of this premise, the pK_a for the met-on to met-off transition appeared to be shifted to a lower pH in pure MES buffer, where the rate is maximized at lower pH (the XAS titration curve could not be fully determined in MES because pHs of <5.0 were not attainable).

An important feature of the met-off form is the fact that the Cu−S distance does not change during the pH transition. This might suggest that the met-on to met-off transition simply involves methionine dissociation. However, several factors argue in favor of the alternative explanation that the Cu−S interaction is still present at 2.25 Å but has become more labile or disordered. In support of this premise, the Cu−S interaction never disappears from the spectra, and at high pH, the DW factor remains constant at 0.012 Å^2. Although fits to the data can be obtained by lowering the Cu−S coordination number (as expected from the correlation between the DW factor and shell occupancy), these fits are quantitatively worse than those where the DW factor is allowed to increase. Further such fits would imply that the methionine coordinates Cu(I) substoichiometrically in the met-off form (even at pH 10), since *N* never reaches zero (Table 3). For these reasons, we prefer to describe the met-off form as one containing a disordered Cu−S bond. Because there is only a single met residue coordinated, this implies a dynamic rather than static disorder, and suggests that the met-off form can sample many conformational states.

The structural origins of the met-on to met-off transition remain unclear, but a preponderance of evidence suggests that protein conformational changes are at work, rather than local effects on the coordination chemistry of the Cu_M center. First, photoreduction of the oxidized protein (where the met ligand is always dissociated and thus in an off configuration) at 100 K in acetate-containing buffer at pH 5 produced a fully met-off form rather than the met-on form expected for the reduced enzyme in acetate buffer at this pH. However, the solvent shell present in oxidized Cu_M was still able to dissociate from the Cu(I) center, showing that the mobility of local ligands around the copper center was not compromised. The failure of the met ligand to bind to Cu(I) therefore implicates a more global protein conformational change which would be prevented in the frozen matrix. Second, formation of the met-off form appears to induce ligand dissociation at the Cu_H center, 11 Å distant, and the recently determined crystal structure of the M314I mutant showed significant structural changes at Cu_H, providing a link between coordination of the methionine residue and the protein structure at a site 11 Å distant (*7*). Third, binding of a peptidylglycine substrate appears to have little or no effect on the position of the met-on−met-off equilibrium, and vice versa, the K_d for peptide binding remains unchanged in the pH range of 5−8. Since substrate binding cross-links the two β-strands that carry Cu_M ligands M314 and H242/H244, K_d^{YVG} would be expected to reflect the on−off transition unless both β-strands could move in unison. Thus binding of substrate does not "lock in" a methionine conformation; rather, the protein dynamics which modulate the methionine coordination appear to include or be transmitted to the substrate.

The methionine ligand is catalytically essential as shown previously from mutagenesis studies (*31*), and various proposals for explaining its critical catalytic role have been advanced. The relatively high values of ν(CO) for the carbonyl complexes of PHM and DBM (2093 and 2089 cm^{-1}, respectively) relative to those of tris-imidazole systems (e.g., hemocyanin, 2043−2063 cm^{-1}) emphasize the fact that the S atom of the thioether ligand is a poor electron donor (*8*, *10*, *40*, *41*). In model systems, the CuN_3 ligand sets (five- or six-membered heterocycle) lead to ν(CO) values lower than those of the corresponding CuN_2S systems due to a decreased level of electron donation from the thioether and consequent decreased level of back-bonding to CO (*42*). It has been suggested (*16*) that this weak donation keeps the $Cu-O_2$ complex electrophilic such that O_2 reduction does not occur until substrate activation by H atom abstraction. In essence, this effect would shift the equilibrium constant for Cu(I)−dioxygen binding to the left, by methionine stabilization of the Cu(I) form, thereby inhibiting uncoupling reactions induced by "leakage" of superoxide or peroxide from the active site (*16*, *26*). A recent study of binding of dioxygen to β-diketiminate−Cu(I) complexes containing a thioether pendant arm has shown little or no influence of the thioether ligand on the electronic description of the ensuing Cu(I)−dioxygen complexes (*43*) which are best formulated as intermediate between Cu(II)−superoxo and Cu(III)−peroxo species (*43*, *44*). However, the thioether coordination appears to increase the reversibility of the system and suggests a small shift in equilibrium in favor of the Cu(I)−O_2 form or an increase in the k_{off} rate for molecular oxygen. The Cu(I) stabilizing role of methionine is also evident in our own studies of the peroxide reactivity of PHM where analysis of product isotopomers clearly shows an equilibrium between Cu(II)−superoxo and Cu(I)−dioxygen species (*29*). These effects probably have their origins in the ability of thioether S donors to form relatively strong and presumably more covalent bonds to the "soft" d^{10} Cu(I) configuration but weaker and longer bonds to Cu(II), where the solvent competes effectively as an electron donor for the "harder" cupric ion.

While rationalizing the electronic trends expected for methionine coordination, this discussion falls short of providing a rationale for the absolute catalytic requirement for methionine coordination. Further, if the essential nature of the met ligand resides in its electronic properties per se, the met-on form might be expected to be most active where the electronic effects would be amplified. However, this work shows clearly that the methionine coordination is coupled to catalytically critical enzyme dynamics. It is unclear whether the fluxional nature of the Cu(I)−methionine interaction drives the protein dynamics, or vice versa. Elevated Cu−S DW factors appear to be present in the

carbon monoxide complexes of PHM and DBM (*10*, *12*, *41*). CO binds to Cu_M in a four-coordinate complex with H242, H244, and M314 as the other ligands. Here the Cu−S distance becomes longer (2.32 Å), a value characteristic of a four-coordinate complex, but the DW factor (0.009 $Å^2$ for PHM and 0.008 $Å^2$ for DBM) is more than twice that of the Cu−C(CO) value. Back-bonding from Cu(I) to CO should increase the positive charge on Cu(I) and thus increase the strength of the Cu−S bond together with its DW factor. It is also intriguing that in the β-diketiminate−thioether−Cu(I) system, NMR shows the presence of two species, a low-temperature multinuclear complex with tight intermolecular Cu−S interactions and a high-temperature species showing fluxional behavior attributed to rapid association and dissociation of the thioether ligand (*43*). It is therefore possible that the protein is using the fluxional properties of the Cu(I)−thioether interaction to modulate the protein dynamics at the active site.

These considerations lead to an alternative hypothesis for the essential role of the methionine ligand. A recent study of intrinsic kinetic isotope effects (KIEs) in the PHM system using ^{2}H-substituted hippuric acid as substrate has provided clear evidence for nonclassical behavior in the H abstraction step; viz. H atom transfer proceeds via a tunneling mechanism (*18*). It is now widely accepted that the rates of H tunneling processes follow rules broadly similar to those of electron tunneling and involve (i) a protein reorganizational energy term (λ) required to match the reaction coordinates of reactant and product prior to H transfer and (ii) a term that describes the probability of H tunneling through the barrier which depends on the overlap of donor and acceptor orbitals (*45*, *46*). As with electron transfer, λ measures the ability of the protein to adopt or sample conformations that render the donor and acceptor orbitals roughly degenerate. The probability term is much more localized as the proton wavelength is short and is usually described in terms of a thermally activated vibration along the reaction coordinate (often termed a gating interaction). Systems dominated by protein conformational dynamics (λ dominates) typically have little or no temperature dependence of the KIEs, while systems which use a thermally accessible vibrational state to increase the probability of tunneling typically exhibit strong a temperature dependence of the KIE.

Analysis of the temperature dependence of the KIEs in the PHM system has predicted that both terms are important in describing the tunneling process (*18*). Specifically, this implies conformational mobility of the substrate relative to the copper−superoxo active species and an accessible vibrational mode modulating the tunneling probability along the Cu−O···H···C coordinate. Physical evidence for the existence of such modes is generally scarce, but XAS-derived Debye−Waller factors provide a rare opportunity to obtain precisely this type of information, since they report on the dynamic displacement of the scatterer from its average position along the absorber scatterer vector. The unusually high value of the DW factor for the Cu−S(met) interaction implies the existence of low-frequency conformational sampling of the protein in the vicinity of Cu_M which exactly tracks the catalytic activity in both buffer systems and, therefore, in all probability is sampling the same protein dynamics which are critical for the tunneling process. This would nicely explain the correlation of Cu−S DW factor and reaction rate.

Close examination of the binding site for substrate shows that it cross-links two β-strands via interactions with R240 on the strand carrying copper ligands H242 and H244, and with Y318 and N316 on the strand carrying M314. Cysteine 315 anchors the latter strand via a disulfide bond. Thus, modulation of the Cu−S(met) interaction would be transmitted to the substrate via a scissor motion of the substrate-binding β-strands about the C315 disulfide anchor and could thus lead to a modulation of the Cu−O···H···C distance.

ACKNOWLEDGMENT

We gratefully acknowledge the use of facilities at the Stanford Synchrotron Radiation Laboratory which is supported by the National Institutes of Health Biomedical Research Technology Program, Division of Research Resources, and by the U.S. Department of Energy, Basic Energy Sciences (BES), and Office of Biological and Environmental Research.

SUPPORTING INFORMATION AVAILABLE

Derivation of equations used to fit the rate−pH profiles, tables of rate−pH data in different buffers, and the complete parameter sets for EXAFS simulations. This material is available free of charge via the Internet at http://pubs.acs.org.

REFERENCES

1. Klinman, J. P. (1996) Mechanisms whereby mononuclear copper proteins functionalize organic substrates, *Chem. Rev. 96*, 2541−2561.
2. Prigge, S. T., Mains, R. E., Eipper, B. A., and Amzel, L. M. (2000) New insights into copper monooxygenases and peptide amidation: Structure, mechanism and function, *Cell. Mol. Life Sci. 57*, 1236−1259.
3. Klinman, J. P. (2006) The copper-enzyme family of dopamine β-monooxygenase and peptidylglycine α-hydroxylating monooxygenase: Resolving the chemical pathway for substrate hydroxylation, *J. Biol. Chem. 281*, 3013−3016.
4. Prigge, S. T., Kolhekar, A. S., Eipper, B. A., Mains, R. E., and Amzel, L. M. (1997) Amidation of bioactive peptides: The structure of peptidylglycine α-hydroxylating monooxygenase, *Science 278*, 1300−1305.
5. Prigge, S. T., Kolhekar, A. S., Eipper, B. A., Mains, R. E., and Amzel, L. M. (1999) Substrate-mediated electron transfer in peptidylglycine α-hydroxylating monooxygenase, *Nat. Struct. Biol. 6*, 976−983.
6. Prigge, S. T., Eipper, B. A., Mains, R. E., and Amzel, M. (2004) Dioxygen binds end-on to mononuclear copper in a precatalytic enzyme complex, *Science 304*, 864−867.
7. Siebert, X., Eipper, B. A., Mains, R. E., Prigge, S. T., Blackburn, N. J., and Amzel, L. M. (2005) The catalytic copper of peptidylglycine α-hydroxylating monooxygenase also plays a critical structural role, *Biophys. J. 89*, 3312−3319.
8. Boswell, J. S., Reedy, B. J., Kulathila, R., Merkler, D. J., and Blackburn, N. J. (1996) Structural investigations on the coordination environment of the active-site copper centers of recombinant bifunctional peptidylglycine α-amidating enzyme, *Biochemistry 35*, 12241−12250.
9. Kolhekar, A. S., Keutman, H. T., Mains, R. E., Quon, A. S. W., and Eipper, B. A. (1997) Peptidylglycine α-hydroxylating monooxygenase: Active site residues, disulfide linkages, and a two-domain model of the catalytuc core, *Biochemistry 36*, 10901−10909.
10. Jaron, S., and Blackburn, N. J. (1999) Does superoxide channel between the copper centers in peptidylglycine monooxygenase? A new mechanism based on carbon monoxide reactivity, *Biochemistry 38*, 15086−15096.

11. Blackburn, N. J., Rhames, F. C., Ralle, M., and Jaron, S. (2000) Major changes in copper coordination accompany reduction of peptidylglycine monooxygenase, *J. Biol. Inorg. Chem. 5*, 341−353.
12. Jaron, S., and Blackburn, N. J. (2001) Characterization of a half-apo derivative of peptidylglycine monooxygenase. Insight into the reactivity of each active site copper, *Biochemistry 40*, 6867−6875.
13. Jaron, S., Mains, R. E., Eipper, B. A., and Blackburn, N. J. (2002) The catalytic role of the copper ligand H172 of peptidylglycine α-hydroxylating monooxygenase (PHM): A spectroscopic study of the H172A mutant, *Biochemistry 41*, 13274−13282.
14. Bell, J., El Meskini, R., D'Amato, D., Mains, R. E., and Eipper, B. A. (2003) Mechanistic investigation of peptidylglycine α-hydroxylating monooxygenase via intrinsic tryptophan fluorescence and mutagenesis, *Biochemistry 42*, 7133−7142.
15. Chen, P., Bell, J., Eipper, B. A., and Solomon, E. I. (2004) Oxygen activation by the noncoupled binuclear copper site in peptidylglycine α-hydroxylating monooxygenase. Spectroscopic definition of the resting sites and the putative $CuII_M$-OOH intermediate, *Biochemistry 43*, 5735−5747.
16. Evans, J. P., Ahn, K., and Klinman, J. P. (2003) Evidence that dioxygen and substrate activation are tightly coupled in dopamine β-monooxygenase: Implications for oxygen activation, *J. Biol. Chem. 278*, 49691−49698.
17. Francisco, W. A., Merkler, D. J., Blackburn, N. J., and Klinman, J. P. (1998) Kinetic mechanism and intrinsic isotope effects for the peptidylglycine α-amidating enzyme reaction, *Biochemistry 37*, 8244−8252.
18. Francisco, W. A., Knapp, M. J., Blackburn, N. J., and Klinman, J. P. (2002) Hydrogen tunneling in peptidylglycine α-hydroxylating monooxygenase, *J. Am. Chem. Soc. 124*, 8194−8195.
19. Francisco, W. A., Blackburn, N. J., and Klinman, J. P. (2003) Oxygen and hydrogen isotope effects in an active site tyrosine to phenylalanine mutant of peptidylglycine α-hydroxylating monooxygenase: Mechanistic implications, *Biochemistry 42*, 1813−1819.
20. Francisco, W. A., Wille, G., Smith, A. J., Merkler, D. J., and Klinman, J. P. (2004) Investigation of the pathway for inter-copper electron transfer in peptidylglycine α-amidating monooxygenase, *J. Am. Chem. Soc. 126*, 13168−13169.
21. Roberts, S. A., Weichsel, A., Grass, G., Thakali, K., Hazzard, J. T., Tollin, G., Rensing, C., and Montfort, W. R. (2002) Crystal structure and electron-transfer kinetics of CueO, a multicopper oxidase required for copper homeostasis in *Escherichia coli*, *Proc. Natl. Acad. Sci. U.S.A. 99*, 2766−2771.
22. Loftin, I. R., Franke, S., Roberts, S. A., Weichsel, A., Heroux, A., Montfort, W. R., Rensing, C., and McEvoy, M. M. (2005) A novel copper-binding fold for the periplasmic copper resistance protein CusF, *Biochemistry 44*, 10533−10540.
23. Arnesano, F., Banci, L., Bertini, I., Mangani, S., and Thompsett, A. R. (2003) A redox switch in CopC: An intriguing copper trafficking protein that binds copper(I) and copper(II) at different sites, *Proc. Natl. Acad. Sci. U.S.A. 100*, 3814−3819.
24. Peariso, K., Huffman, D. L., Penner-Hahn, J. E., and O'Halloran, T. V. (2003) The PcoC copper resistance protein coordinates Cu(I) via novel S-methionine interactions, *J. Am. Chem. Soc. 125*, 342−343.
25. Wernimont, A. K., Huffman, D. L., Finney, L. A., Demeler, B., O'Halloran, T. V., and Rosenzweig, A. C. (2003) Crystal structure and dimerization equilibria of PcoC, a methionine-rich copper resistance protein from *Escherichia coli*, *J. Biol. Inorg. Chem. 8*, 185−194.
26. Chen, P., and Solomon, E. I. (2004) Oxygen activation by the noncoupled binuclear copper site in peptidylglycine α-hydroxylating monooxygenase. Reaction mechanism and role of the noncoupled nature of the active site, *J. Am. Chem. Soc. 126*, 4991−5000.
27. Gerdemann, C., Eicken, C., and Krebs, B. (2002) The crystal structure of catechol oxidase: New insight into the function of type-3 copper proteins, *Acc. Chem. Res. 35*, 183−191.
28. Chen, P., and Solomon, E. I. (2004) O_2 activation by binuclear Cu sites: Noncoupled versus exchange coupled reaction mechanisms, *Proc. Natl. Acad. Sci. U.S.A. 101*, 13105−13110.
29. Bauman, A. T., Yukl, E. T., Alkevich, K., McCormack, A. L., and Blackburn, N. J. (2006) The hydrogen peroxide reactivity of peptidylglycine monooxygenase supports a Cu(II)-superoxo catalytic intermediate, *J. Biol. Chem. 281*, 4190−4198.
30. Kamachi, T., Kihara, N., Shiota, Y., and Yoshizawa, K. (2005) Computational exploration of the catalytic mechanism of dopamine β-monooxygenase: Modeling of its mononuclear copper active sites, *Inorg. Chem. 44*, 4226−4236.
31. Eipper, B. A., Quon, A. S. W., Mains, R. E., Boswell, J. S., and Blackburn, N. J. (1995) The catalytic core of peptidylglycine α-hydroxylating monooxygenase: Investigation by site-directed mutagenesis, Cu X-ray absorption spectroscopy, and electron paramagnetic resonance, *Biochemistry 34*, 2857−2865.
32. George, G. N. (1990) *EXAFSPAK*, Stanford Synchrotron Radiation Laboratory, Menlo Park, CA.
33. Binsted, N., Gurman, S. J., and Campbell, J. W. (1998) *EXCURVE*, version 9.2, Daresbury Laboratory, Warrington, England.
34. Gurman, S. J., Binsted, N., and Ross, I. (1984) A rapid, exact, curved-wave theory for EXAFS calculations, *J. Phys. C 17*, 143−151.
35. Gurman, S. J., Binsted, N., and Ross, I. (1986) A rapid, exact, curved-wave theory for EXAFS calculations. II. The multiple-scattering contributions, *J. Phys. C 19*, 1845−1861.
36. Binsted, N., and Hasnain, S. S. (1996) State of the art analysis of whole X-ray absorption spectra, *J. Synchrotron Radiat. 3*, 185−196.
37. Sanyal, I., Karlin, K. D., Strange, R. W., and Blackburn, N. J. (1993) Chemistry and structural studies on the dioxygen-binding copper 1,2-dimethylimidazole system, *J. Am. Chem. Soc. 115*, 11259−11270.
38. Kau, L. S., Spira-Solomon, D., Penner-Hahn, J. E., Hodgson, K. O., and Solomon, E. I. (1987) X-ray absorption edge determination of the oxidation state and coordination number of copper: Application to the type 3 site in *Rhus vernicifera* laccase and its reaction with oxygen, *J. Am. Chem. Soc. 109*, 6433−6422.
39. Blackburn, N. J., Strange, R. W., Reedijk, J., Volbeda, A., Farooq, A., Karlin, K. D., and Zubieta, J. (1989) X-ray absorption edge spectroscopy of copper(I) complexes. Coordination geometry of copper(I) in the reduced forms of copper proteins and their derivatives with carbon monoxide, *Inorg. Chem. 28*, 1349−1357.
40. Blackburn, N. J., Pettingill, T. M., Seagraves, K. S., and Shigeta, R. T. (1990) Characterization of a carbon monoxide complex of reduced dopamine-β-hydroxylase: Evidence for inequivalence of the Cu(I) centers, *J. Biol. Chem. 265*, 15383−15386.
41. Pettingill, T. M., Strange, R. W., and Blackburn, N. J. (1991) Carbonmonoxy dopamine-β-hydroxylase: Structural characterization by FTIR, fluorescence and XAS spectroscopy, *J. Biol. Chem. 266*, 16996−17003.
42. Sorrell, T. N., and Borovick, A. S. (1987) Absorption, emission, and photophysical properties of copper(I) pyrazole complexes and their carbonyl adducts, *Inorg. Chem. 26*, 1957−1964.
43. Aboelella, N. W., Gherman, B. F., Hill, L. M., York, J. T., Holm, N., Young, V. G., Jr., Cramer, C. J., and Tolman, W. B. (2006) Effects of thioether substituents on the O_2 reactivity of β-diketiminate-Cu(I) complexes: Probing the role of the methionine ligand in copper monooxygenases, *J. Am. Chem. Soc. 128*, 3445−3458.
44. Aboelella, N. W., Kryatov, S. V., Gherman, B. F., Brennessel, W. W., Young, V. G., Jr., Sarangi, R., Rybak-Akimova, E. V., Hodgson, K. O., Hedman, B., Solomon, E. I., Cramer, C. J., and Tolman, W. B. (2004) Dioxygen activation at a single copper site: Structure, bonding, and mechanism of formation of 1:1 Cu−O_2 adducts, *J. Am. Chem. Soc. 126*, 16896−16911.
45. Knapp, M. J., and Klinman, J. P. (2002) Environmentally coupled hydrogen tunneling. Linking catalysis to dynamics, *Eur. J. Biochem. 269*, 3113−3121.
46. Klinman, J. P. (2006) The role of tunneling in enzyme catalysis of C−H activation, *Biochim. Biophys. Acta* (in press).

BI060905A